J|A|C|S
ARTICLES
Published on Web 04/11/2006

Functional Dynamics of Human FKBP12 Revealed by Methyl ^{13}C Rotating Frame Relaxation Dispersion NMR Spectroscopy

Ulrika Brath,[†] Mikael Akke,[†] Daiwen Yang,[‡,§] Lewis E. Kay,[‡] and Frans A. A. Mulder*[,†,⊥]

Contribution from the Department of Biophysical Chemistry, Lund University, Box 124, SE-221 00 Lund, Sweden, and the Departments of Medical Genetics, Biochemistry, and Chemistry, The University of Toronto, Toronto, Ontario M5S 1A8, Canada

Received October 15, 2005; E-mail: f.a.a.mulder@rug.nl

Abstract: Transverse relaxation dispersion NMR spectroscopy can provide atom-specific information about time scales, populations, and the extent of structural reorganization in proteins under equilibrium conditions. A method is described that uses side-chain methyl groups as local reporters for conformational transitions taking place in the microsecond regime. The experiment measures carbon nuclear spin relaxation rates in the presence of continuous wave off-resonance irradiation, in proteins uniformly enriched with ^{13}C, and partially randomly labeled with ^{2}H. The method was applied to human FK-506 binding protein (FKBP12), which uses a common surface for binding substrates in its dual role as both an immunophilin and folding assistant. Conformational dynamics on a time scale of ~130 μs were detected for methyl groups located in the substrate binding pocket, demonstrating its plasticity in the absence of substrate. The spatial arrangement of affected side-chain atoms suggests that substrate recognition involves the rapid relative movement of the subdomain comprising residues Ala81-Thr96 and that the observed dynamics play an important role in facilitating the interaction of this protein with its many partners, including calcineurin.

Introduction

Protein dynamics are critical for biological function. Processes such as folding, ligand binding, enzyme catalysis, and molecular recognition all involve motions that cover a wide range of time scales and amplitudes.[1−6] These processes typically involve transitions to sparsely populated but functionally important states, the detailed characterization of which dramatically improves our understanding of biological function at the molecular level. Nuclear magnetic resonance spectroscopy (NMR) is uniquely suited to study dynamic processes in proteins on a wide range of time scales, and with atomic resolution.[7] For example, chemical or conformational exchange processes on μs−ms time scales introduce a stochastic time dependence into NMR frequencies, that adds an amount R_{ex} to the intrinsic relaxation rates of transverse magnetization ($R_{2,0}$).[8] The conformational exchange contribution to relaxation depends, in addition, on the strength of applied radio frequency (RF) fields, implemented either as CPMG (Carr−Purcell−Meiboom−Gill) refocusing pulse trains, or continuous-wave spin-locks ($R_{1\rho}$).[8] A plot of R_2 as a function of the effective RF field strength forms a relaxation dispersion profile, from which the rates, populations, and chemical shifts of the interconverting conformations are obtained by model fitting. In principle, NMR spectroscopy offers the possibility to monitor conformational exchange processes at all protein backbone and side-chain positions, provided that suitable stable isotopes (e.g., ^{13}C, ^{15}N) have been incorporated. While the majority of experiments reported to date have focused on the main chain,[9−13] a subset of experiments have emerged also for side chains.[14−17] These novel techniques have particularly targeted methyl groups, since their rapid three-fold rotation results in narrow spectral lines and therefore yields high-quality spectra even for larger proteins.[18,19] In addition, methyl-containing amino acid residues

[†] Lund University.
[‡] The University of Toronto.
[§] Present address: Department of Biological Sciences, National University of Singapore, Science Drive 4, Singapore 117543.
[⊥] Present address: Department of Biophysical Chemistry, University of Groningen, Nijenborgh 4, 9747 AG Groningen, the Netherlands.

(1) Malmendal, A.; Evenäs, J.; Forsén, S.; Akke, M. *J. Mol. Biol.* **1999**, *293*, 883−899.
(2) Lee, A. L.; Kinnear, S. A.; Wand, A. J. *Nat. Struct. Biol.* **2000**, *7*, 72−77.
(3) Mulder, F. A. A.; Mittermaier, A.; Hon, B.; Dahlquist, F. W.; Kay, L. E. *Nat. Struct. Biol.* **2001**, *8*, 932−935.
(4) Eisenmesser, E. Z.; Bosco, D. A.; Akke, M.; Kern, D. *Science* **2002**, *295*, 1520−1523.
(5) Korzhnev, D. M.; Salvatella, X.; Vendruscolo, M.; Di Nardo, A. A.; Davidson, A. R.; Dobson, C. M.; Kay, L. E. *Nature* **2004**, *430*, 586−590.
(6) Wolf-Watz, M.; Thai, V.; Henzler-Wildman, K.; Hadjipavlou, G.; Eisenmesser, E. Z.; Kern, D. *Nat. Struct. Mol. Biol.* **2004**, *11*, 945−949.
(7) Palmer, A. G. *Annu. Rev. Biophys. Biomol. Struct.* **2001**, *30*, 129−155.
(8) Palmer, A. G.; Kroenke, C. D.; Loria, J. P. *Methods Enzymol.* **2001**, *339*, 204−238.
(9) Akke, M.; Palmer, A. G. *J. Am. Chem. Soc.* **1996**, *118*, 911−912.
(10) Loria, J. P.; Rance, M.; Palmer, A. G. *J. Am. Chem. Soc.* **1999**, *121*, 2331−2332.
(11) Ishima, R.; Wingfield, P. T.; Stahl, S. J.; Kaufman, J. D.; Torchia, D. A. *J. Am. Chem. Soc.* **1998**, *120*, 10534−10542.
(12) Mulder, F. A. A.; Akke, M. *Magn. Reson. Chem.* **2003**, *41*, 853−865.
(13) Lundström, P.; Akke, M. *J. Biomol. NMR* **2005**, *32*, 163−173.
(14) Ishima, R.; Louis, J. M.; Torchia, D. A. *J. Am. Chem. Soc.* **1999**, *121*, 11589−11590.
(15) Mulder, F. A. A.; Skrynnikov, N. R.; Hon, B.; Dahlquist, F. W.; Kay, L. E. *J. Am. Chem. Soc.* **2001**, *123*, 967−975.
(16) Mulder, F. A. A.; Hon, B.; Mittermaier, A.; Dahlquist, F. W.; Kay, L. E. *J. Am. Chem. Soc.* **2002**, *124*, 1443−1451.
(17) Skrynnikov, N. R.; Mulder, F. A. A.; Hon, B.; Dahlquist, F. W.; Kay, L. E. *J. Am. Chem. Soc.* **2001**, *123*, 4556−4566.

10.1021/ja0570279 CCC: $33.50

are ubiquitous in proteins and provide a large number of probes distributed throughout the three-dimensional structure. Furthermore, methyl groups often are localized to hydrophobic crevices or surface patches involved in protein−ligand or protein−protein interactions.[2,20] The above qualities make the ^{13}C spins of methyl groups particularly suitable for studying conformational dynamics associated with ligand binding and enzyme catalysis.

Here we present a new experiment directed at methyl groups to quantitatively analyze rapid (μs time scale) structural transitions. In this approach off-resonance ^{13}C $R_{1\rho}$ relaxation dispersion profiles are measured for $^{13}CHD_2$ methyl isotopomers in protein samples with uniform ^{13}C- and random fractional ^{2}H-labeling. There are a number of key advantages to this avenue. First, protein samples produced with the isotopic enrichment mentioned above are commonly prepared for structural and dynamics studies by NMR[21] and are therefore cost-effective to produce. Second, the use of spin-lock measurements[14] permits faster processes to be monitored at methyl positions than CPMG-based methods.[14,16,17] Third, the 2.5 times larger magnetogyric ratio for carbon-13 compared to nitrogen-15 allows processes with rates that are faster to be studied at a given RF power level, with ^{13}C as opposed to ^{15}N $R_{1\rho}$ relaxation dispersion spectroscopy. Fourth, selective detection of $^{13}CHD_2$ isotopomers ensures that the intrinsic ^{13}C relaxation rates (i.e., in the absence of chemical exchange) are very low so that small relaxation contributions from μs time scale motions can be accurately detected and quantitatively analyzed. Cross-correlated dipolar spin relaxation contributions between pairs of methyl $^{13}C-^{1}H$ spins are eliminated, thereby facilitating the interpretation of the relaxation data in terms of chemical exchange processes. In principle uniform enrichment with carbon ensures that all methyl groups in the protein are available for analysis. However, this advantage is partially offset by potential complications arising from isotropic mixing among carbon spins during spin-lock RF irradiation. A comprehensive examination shows that homonuclear Hartmann−Hahn matching does not compromise relaxation measurement for the majority of methyl groups, thereby enabling accurate analysis of chemical exchange contributions.

We applied the off-resonance ^{13}C $R_{1\rho}$ relaxation measurement to human FK-506 binding protein (FKBP12), and demonstrated that conformational dynamics in this protein occur principally at the binding surface for immunosuppressant and peptide substrates. A small subdomain, comprising residues Ala81-Thr96, appears to form a moveable flank that brings residues into place for the interaction with FK-506 substrate and to create a joint surface for calcineurin recognition and immunosuppressant action. Moreover, the high plasticity that is associated with this region is likely to be key in the ability of FKBP12 to bind to the large number of targets that have been identified. Finally, we discuss alternative labeling strategies that would reduce or avoid Hartmann−Hahn matching and that provide benefits in applications involving high-molecular weight proteins and their complexes.

Theory

Relaxation of ^{13}C in CHD_2 with ^{13}C Irradiation. In the specific case of an isolated AX spin system, the rotating-frame relaxation rate of a locked spin (^{15}N or ^{13}C in the context of $^{15}N-^{1}H$ or $^{13}C-^{1}H$ spin systems, for example) is given by[8]

$$R_{1\rho} = R_1 \cos^2\theta + R_{2,0} \sin^2\theta + R_{ex} \sin^2\theta \qquad (1)$$

where R_1 and $R_{2,0}$ are the longitudinal and transverse relaxation rates, respectively, due to dipolar and chemical shift anisotropy interactions, and R_{ex} is the exchange contribution to the transverse relaxation rate R_2 ($R_2 = R_{2,0} + R_{ex}$). Exchange is assumed to occur between two states, A and B, with resonance frequencies ω_A and ω_B, and populations p_A and p_B; the rate of transition from state i to state j is k_{ij} ($i,j = A,B$). The rate of exchange between states is $k_{ex} = k_{AB} + k_{BA}$, which equals the inverse of the mean lifetime of the two states, τ_{ex}. In the presence of an RF field of strength $\omega_1 = -\gamma B_1$, the nuclear spin magnetization that is aligned with the effective field $\omega_{eff} = (\Omega^2 + \omega_1^2)^{1/2}$, (where $\Omega = p_A\omega_A + p_B\omega_B - \omega_c$ is the population-weighted offset from the carrier frequency, ω_c) will be oriented at an angle $\theta = \arctan(\omega_1/\Omega)$ from the static magnetic field. In the case of fast exchange, $k_{ex} \gg \Delta\omega = |\omega_A - \omega_B|$, which is of interest here, R_{ex} for the aligned magnetization is[22, 23]

$$R_{ex} = \phi \frac{k_{ex}}{k_{ex}^2 + \omega_{eff}^2} \qquad (2)$$

where $\phi = p_A p_B (\Delta\omega)^2$. Thus, exchange-mediated transverse relaxation manifests itself by an *additional* dependence on the tilt angle through $\omega_{eff} = \omega_1/\sin\theta$. The free precession limit broadening is given by $R_{ex}(\omega_{eff} \rightarrow 0) = \phi/k_{ex}$.

In the case of applications to more complex spin systems of the AX_2 or AX_3 variety, for example, the relaxation can be decidedly nonexponential due to dipolar cross-correlation. Such effects also depend on the orientation of the spin lock field[24] in a way that would complicate the interpretation of $R_{1\rho}(\theta)$ in terms of exchange. Unlike cross-correlations involving dipolar/CSA fields, $^{1}H-^{13}C$ dipolar cross-correlation effects cannot be eliminated through the application of pulses. The use of $^{13}CHD_2$ methyls (as opposed to $^{13}CH_3$ groups) eliminates complications from interacting $^{1}H-^{13}C$ spin pairs so that, at least in the case of an isolated methyl, it is possible to consider the $^{13}CHD_2$ methyl as an AX spin system to good accuracy.

In practice, however, the labeling scheme that is employed does not produce isolated methyls; rather, the uniform ^{13}C incorporation ensures that each methyl carbon is dipolar (and scalar, see below) coupled to its neighbor. The cross-relaxation between dipolar coupled pairs depends on the orientation of each of the locked spins (i.e., both the methyl and its adjacent carbon) relative to the static magnetic field,[24] and this orientation changes as a function of carrier position. This potentially complicates the extraction of exchange parameters from the orientation dependence of $R_{1\rho}$. Simulations for all of the methyl-containing residues using offsets, spin-lock fields, and spin-

(18) Kay, L. E.; Bull, T. E.; Nicholson, L. K.; Griesinger, C.; Schwalbe, H.; Bax, A.; Torchia, D. A. *J. Magn. Reson.* **1992**, *100*, 538−558.
(19) Hajduk, P. J.; Augeri, D. J.; Mack, J.; Mendoza, R.; Yang, J.; Betz, S. F.; Fesik, S. W. *J. Am. Chem. Soc.* **2000**, *122*, 7898−7904.
(20) Kay, L.; Muhandiram, D.; Wolf, G.; Shoelson, S.; Forman-Kay, J. *Nat. Struct. Biol.* **1998**, *5*, 156−163.
(21) Gardner, K. H.; Kay, L. E. *Annu. Rev. Biophys. Biomol. Struct.* **1998**, *27*, 357−406.
(22) Desvaux, H.; Birlirakis, N.; Wary, C.; Berthault, P. *Mol. Phys.* **1995**, *86*, 1059−1073.
(23) Davis, D. G.; Perlman, M. E.; London, R. E. *J. Magn. Reson., Ser. B* **1994**, *104*, 266−275.
(24) Bull, T. *Prog. Nucl. Magn. Reson. Spectrosc.* **1992**, *24*, 377−410.

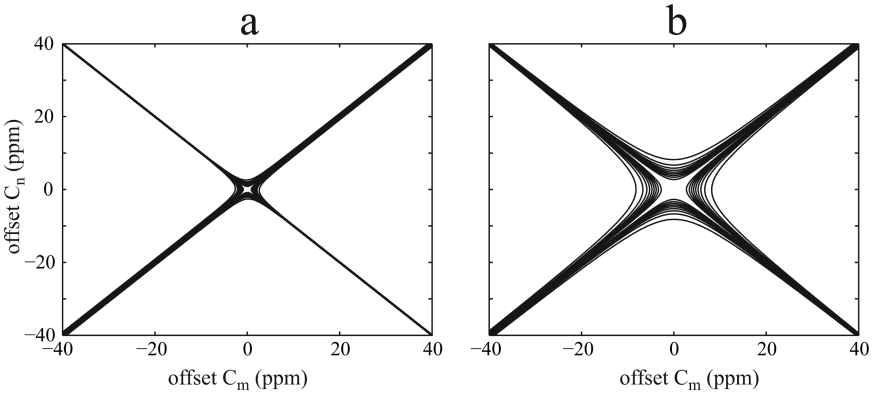

Figure 1. Efficiency of Hartmann−Hahn coherence transfer of magnetization between carbon spins under continuous wave irradiation. The amplitude of in-phase Hartmann−Hahn coherence transfer, A_{HaHa}, is plotted as a function of the offsets of the resonance frequencies of two adjacent scalar-coupled nuclei from the spin-lock carrier, with $^1J_{CC} = 35$ Hz. The RF field has a frequency $\omega_c/2\pi = 125$ MHz and field strength $\gamma B_1/2\pi = 0.5$ and 5.0 kHz in panels a and b, respectively. Complete Hartmann−Hahn matching, corresponding to $A_{HaHa} = 1.0$, occurs along the diagonal and anti-diagonal. Contour levels are shown from 0.9 to 0.1, in 0.1 decrements, with A_{HaHa} falling off away from the (anti)diagonal.

lock times that have been implemented experimentally establish, however, that such offset-dependent cross-relaxation terms are sufficiently small, so that they have essentially no effect on the robust extraction of exchange parameters. It is worth noting, however, that cross-relaxation effects can be reduced even further (from their already very small contributions) by careful design of the experiment so that at the start of the spin-lock period magnetization from the methyl spin only is present (i.e. the initial magnetization of the adjacent ^{13}C spin is zero, see below). In this manner, relaxation of the methyl spin of interest proceeds in an exponential manner for an extended period. In what follows all of the dispersion data recorded on $^{13}CHD_2$ groups from FKBP12 labeled uniformly with ^{13}C and fractionally with ^{2}H has been interpreted using eq 1.

Coherent Magnetization Transfer During ^{13}C Irradiation. Hartmann−Hahn matching of the effective fields experienced by two coupled spins induces magnetization transfer between them, which interferes with the measurement of accurate relaxation rates. For two coupled carbon spins, *I* and *S*, the effectiveness of Hartmann−Hahn matching is given[25] by the coherence transfer function

$$F_{\mathrm{HaHa}} = \frac{1}{1 + (\Delta/J_{\mathrm{eff}})^2}\sin^2(DT/2) = A_{\mathrm{HaHa}}\sin^2(DT/2) \quad (3)$$

where $D = (\Delta^2 + J_{\mathrm{eff}}^2)^{1/2}$, $\Delta = \omega_{\mathrm{eff,I}} - \omega_{\mathrm{eff,S}}$, $J_{\mathrm{eff}} = J(1 + \cos(\theta_I - \theta_S))/2$, J is the scalar-coupling constant (in *angular* frequency units), and T is the length of the spin-lock period. The meaning of the other symbols is explained in the previous section. Figure 1 shows simulations of the coherence transfer amplitude, A_{HaHa}, as a function of offset for two spins when the spin-lock field strength is 0.5 kHz (a) or 5.0 kHz (b). Since A_{HaHa} depends strongly on the offset, continuous wave irradiation is a very poor scheme for isotropic mixing when (1) the chemical shifts of the spins are distinct and when (2) the carrier does not lie between the resonance frequencies of the scalar-coupled spins. Interestingly, as can be seen in Figure 1a, A_{HaHa} decreases more steeply as a function of the difference in offset for $\theta_I = (180° - \theta_S)$ than for $\theta_I = \theta_S$, due to a more rapid falloff of J_{eff}.

(25) van de Ven, F. J. M. *Multidimensional NMR in liquids. Basic principles and experimental methods*; Wiley-VCH: New York, 1995; p 399.

Materials and Methods

Sample Preparation. Recombinant human FKBP12 ($M_r = 11.8$ kDa; EC 5.2.1.8), uniformly enriched with ^{13}C and ^{15}N and fractionally deuterated, was produced by overexpression in *Escherichia coli* BL21* with ^{13}C-glucose and $^{15}NH_4Cl$ as the sole carbon and nitrogen sources, and with 50% v/v D_2O in the culture medium. The cell lysate was applied to a CM cellulose column equilibrated with 10 mM Tris buffer, 1mM EDTA, and 1 mM DTT, and eluted with a linear gradient of 0−0.5 M NaCl. Following lyophilization, the protein was desalted on a Sephadex G25 gel filtration column. The NMR sample contained 1.5 mM protein dissolved in 25 mM potassium phosphate, 90%/10% v/v H_2O/D_2O at pH 7.0, with trace amounts of 2,2-dimethyl-2-silapentane-5-sulfonic acid (DSS) and NaN_3. ^{15}N labeling is not necessary for the experiments described herein but makes it possible to monitor ^{15}N and ^{13}C relaxation under identical conditions, which provides a valuable point of reference. For assignment purposes a uniformly ^{13}C−^{15}N-labeled sample was also produced. To obtain stereospecific methyl assignments one culture was grown on a mixture of 10% U-^{13}C-labeled and 90% unlabeled glucose to make use of the stereospecific pyruvate biosynthesis pathways of *E. coli*.[26]

NMR Spectroscopy. NMR relaxation and chemical shift assignment experiments were performed at 20 °C on Varian Inova spectrometers operating at 500 and 600 MHz ^{1}H frequency, respectively. A triple-resonance probe head with pulsed field-gradient capabilities was employed. Previous ^{15}N backbone assignments of FKBP12 were confirmed by recording a 3D ^{1}H−^{15}N TOCSY-HSQC.[27,28] Side-chain ^{1}H chemical shifts were correlated with $^{13}C^{\alpha}$ and side-chain ^{13}C resonance frequencies of methyl-containing residues using a 3D HCCH-TOCSY spectrum.[29] Stereospecific assignments for Leu and Val residues were obtained from a constant-time (CT) ^{1}H−^{13}C HSQC spectrum[30] acquired on the 10% ^{13}C-labeled sample. Distinction of the pro-*S* and pro-*R* methyl groups was based on the signs of cross-peaks in the CT-HSQC spectrum, relative to the ϵ-methyl group of Met (which has no ^{13}C neighbor).

Pulse Sequence. $R_{1\rho}$ relaxation rates were measured using the pulse scheme shown in Figure 2. Narrow (wide) filled bars indicate 90° (180°) RF pulses applied with phase *x*, unless otherwise indicated. Filled rectangular ^{1}H pulses are applied with a field strength of $\omega_1/2\pi = 30$

(26) Neri, D.; Szyperski, T.; Otting, G.; Senn, H.; Wüthrich, K. *Biochemistry* **1989**, *28*, 7510−7516.
(27) Zuiderweg, E. R. P.; Fesik, S. *Biochemistry* **1989**, *28*, 2387−2391.
(28) Marion, D.; Kay, L. E.; Sparks, S. W.; Torchia, D. A.; Bax, A. *J. Am. Chem. Soc.* **1989**, *111*, 1515−1517.
(29) Baldisseri, D. M.; Pelton, J. G.; Sparks, S. W.; Torchia, D. A. *FEBS Lett.* **1991**, *281*, 33−38.
(30) van de Ven, F.; Phillipens, M. *J. Magn. Reson.* **1992**, *97*, 637−644.

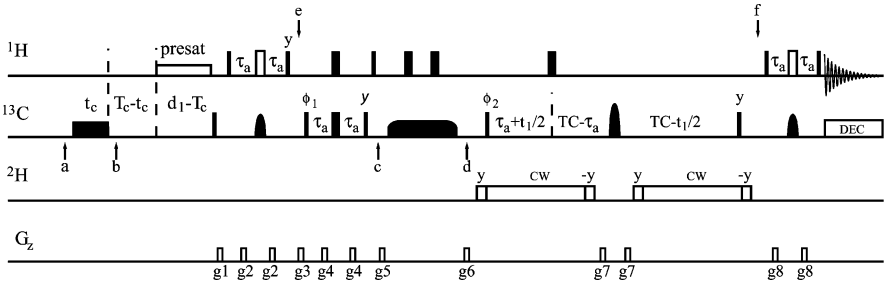

Figure 2. Pulse sequence for the $^{13}CHD_2$-selected off-resonance $R_{1\rho}$ relaxation experiment. Details are given in Materials and Methods.

kHz. The ^{1}H carrier is centered at the water resonance (4.75 ppm), except between points e and f, where it is placed in the methyl region (0.8 ppm). The open rectangle marked "presat" represents weak ($\omega_1/2\pi = 50$ Hz) continuous-wave (cw) irradiation to saturate the solvent water resonance. Empty rectangles represent 180° pulses that are applied at 0.8 ppm by phase modulation. Rectangular ^{13}C pulses are centered at 20 ppm, and applied with $\omega_1/2\pi = 15.2$ kHz. Dome-shaped pulses indicate band-selective REBURP 180° pulses.[31] During the INEPT transfer periods these are applied with peak field strength of $\omega_1/2\pi = 4.2$ kHz and pulse length of 1500 μs, so as to refocus the methyl region exclusively (bandwidth = 20 ppm). The REBURP pulse in the middle of the t_1 evolution period is applied in the center of the aliphatic region (45 ppm) by phase modulation, with peak RF field strength of $\omega_1/2\pi = 16.2$ kHz and pulse length of 390 μs, so as to cover all aliphatic carbon spins (bandwidth 80 ppm). At point c, the carrier is switched to the desired offset of the spin-lock field. The shaped ^{13}C pulse between g_5 and g_6 is the cw spin-lock, flanked by adiabatic rotations (vide infra). ^{1}H 180° pulses during the relaxation delay T (at $T/4$ and $3T/4$) suppress *net* cross relaxation between methyl ^{1}H and ^{13}C spins, as well as interference between ^{13}C CSA/^{13}C−^{1}H dipolar relaxation interactions to second order in time.[14,32] Although in principle ^{13}C CSA/^{13}C−^{2}H dipolar contributions are not directly suppressed, such effects are minimized quite naturally by ^{2}H spin flips (resulting from the ^{2}H quadrupolar interaction) that occur with a rate that is larger than the cross-relaxation rate resulting from the cross-correlated relaxation. ^{13}C Decoupling during acquisition is achieved by GARP-1,[33] with $\omega_1/2\pi = 1.9$ kHz. ^{2}H Decoupling is performed with cw irradiation, using $\omega_1/2\pi = 0.7$ kHz, and with the carrier placed in the center of the methyl region (0.9 ppm). Flanking 90° pulses are given at the same field strength and frequency. Values of the delays are: $\tau_a = 1.98$ ms, $T_c = 14.0$ ms, and $d_1 = 2.0$ s. Gradient strengths in G/cm (lengths in ms) are: $g_1 = 5.0$ (0.5), $g_2 = 3.0$ (0.3), $g_3 = 15.0$ (1.0), $g_4 = 6.0$ (0.3), $g_5 = 10.0$ (1.0), $g_6 = 10.0$ (1.0), $g_7 = 15.0$ (0.2), $g_8 = 9.0$ (0.3). Phase cycling: $\phi_1 = [x,-x]$, $\phi_2 = 2[x]$, $2[-x]$, $\phi_{rec} = [x]$, $2[-x]$, $[x]$. Concomitant inversion of ϕ_1 and the receiver phase ensures that the signal decays to zero.[34] Phase-sensitive 2D spectra were recorded using States-TPPI incrementation[35] of ϕ_2. R_1 relaxation rates were measured using the same pulse sequence (Figure 2), but the central cw spin-lock was omitted. A heat compensation element (between points a and b in the sequence) was used to ensure equal RF deposition as in the $R_{1\rho}$ experiments. Seventeen data points were acquired, including four duplicates, covering $T = 0-400$ ms. $R_{1\rho}$ relaxation rates were measured using 9−10 points per decay curve, covering relaxation delays $T = 0-200$ ms, including one duplicate at $T = 0$ ms. Twelve spin-lock field strengths were used covering the range $\omega_1/2\pi = 506-4511$ Hz. The field strength was calibrated by measuring residual $^1J_{CH}$ splittings in the ^{1}H dimension of a ^{1}H−^{13}C CT-HSQC, acquired with continuous-wave ^{13}C decoupling, as described previously,[12] with an error of 2%. The different spin-lock field strengths were combined with offsets ranging from 1.5 kHz upfield to 5 kHz downfield of the center of the methyl region (exact values are reported in Supporting Information), resulting in 61 data points per dispersion curve, including the R_1 data point. Each data set comprised 64 × 512 complex points ($F_1 \times F_2$), with spectral widths of 2500 and 8000 Hz, respectively. The total acquisition time for each spectrum was approximately 15 min.

Heat Compensation. Because of the variation in both the length of the relaxation delay and in the power of the spin-lock field strength, sample heating can vary from one experiment to the next. Therefore, a heat compensation element was introduced during the delay between scans, while keeping the recycle delay, d_1, constant. The cw compensation field was applied with the same strength as the spin-lock, and, although not necessary, the carrier between points a and b was moved 100 kHz from the methyl resonances. The value of the delays t_c and T_c are calculated in the pulse sequence from the values of the spin-lock length according to Wang and Bax[36] so that the same amount of electric heat dissipation occurs for each value of the spin-lock length. Although it would be more rigorous to compensate also for the different B_1 field strengths used in different experiments, we have not done so here, because with a duty cycle < 10% (maximum spin-lock period of 200 ms and a reasonably long recycle delay of 2 s), the average field was always below 0.4 kHz, and the increase in sample temperature was < 1 °C.

Adiabatic Alignment. The carrier position of the spin-lock field was swept by simultaneous amplitude and phase modulation, using a tanh/tan adiabatic alignment scheme.[37−39] The RF field is swept for a duration of 6 ms, beginning 30 kHz upfield of the methyl region. The key to the success of this approach is to ensure that the sweep does not pass through the resonances of interest too rapidly. When the sweep is too fast, the magnetization cannot follow the changing effective field and instead will start precessing around it, effectively sweeping out a large cone, in violation of the adiabatic condition (see, for example, Hennel and Klinowski[40]). Numerical simulations indicate that the alignment scheme employed here violates the adiabatic condition for those spins that resonate further upfield (i.e. closer to the starting point of the frequency sweep) than approximately $0.9|\omega_1|$ from the spin-lock carrier frequency, i.e., $\Omega < -0.9|\omega_1|$. Therefore, relaxation data points obtained for $\Omega < -0.9|\omega_1|$ were excluded a priori from analysis. Generally the alignment is better than 99%. The maximum deviation occurs for the lowest RF field strength, $\omega_1/2\pi = 506$ Hz, where for resonance frequencies in the vicinity of $\Omega = -506$ Hz (i.e, for spins that are approximately 500 Hz upfield from the carrier position) simulations show that the *z*-component of magnetization oscillates by ±10%. These oscillations rapidly die out due to RF inhomogeneity and only slightly affect the sensitivity of the method.[39] The frequency range that

(31) Geen, H.; Freeman, R. *J. Magn. Reson.* **1991**, *93*, 93−141.
(32) Massi, F.; Johnson, E.; Wang, C.; Rance, M.; Palmer, A., III. *J. Am. Chem. Soc.* **2004**, *126*, 2247−2256.
(33) Shaka, A. J.; Barker, P. B.; Freeman, R. *J. Magn. Reson.* **1985**, *64*, 547−552.
(34) Sklenar, V.; Torchia, D.; Bax, A. *J. Magn. Reson.* **1987**, *73*, 375−379.
(35) Marion, D.; Ikura, M.; Tschudin, R.; Bax, A. *J. Magn. Reson.* **1989**, *85*, 393−399.
(36) Wang, A. C.; Bax, A. *J. Biomol. NMR* **1993**, *3*, 715−720.
(37) Ugurbil, K.; Garwood, M.; Rath, A. R. *J. Magn. Reson.* **1988**, *80*, 448−469.
(38) Garwood, M.; Ke, Y. *J. Magn. Reson.* **1991**, *94*, 511−525.
(39) Mulder, F. A. A.; de Graaf, R. A.; Kaptein, R.; Boelens, R. *J. Magn. Reson.* **1998**, *131*, 351−357.
(40) Hennel, J. W.; Klinowski, J. *Fundamentals of Nuclear Magnetic Resonance*; Longman Scientific & Technical: Essex, UK, 1995.

Table 1. Average Chemical Shifts of Carbon Nuclei in, or Scalar Coupled to, Methyl Carbons[a]

residue	C^{methyl}	shift (ppm)	$^1J_{CC}$	shift (ppm)	$^2J_{CC}$[b]	shift (ppm)	$^3J_{CC}$[b]	shift (ppm)
Ala	β	18.9 ± 1.9	α	53.2 ± 2.0	−		−	
Thr	$\gamma 2$	21.5 ± 1.3	β	69.6 ± 2.1	α	62.2 ± 2.7	−	
Met	ϵ	17.2 ± 2.5	−	−	γ	32.0 ± 1.3	β	33.0 ± 2.3
Val	$\gamma 1/\gamma 2$ upfield	20.3 ± 1.5	β	32.6 ± 1.8	α	62.5 ± 3.0	−	
	$\gamma 1/\gamma 2$ downfield	22.6 ± 1.4	β	32.6 ± 1.8	α	62.5 ± 3.0	−	
Ile	$\delta 1$	13.5 ± 1.8	$\gamma 1$	27.7 ± 2.0	β	38.6 ± 2.1	α	61.6 ± 2.8
							$\gamma 2$	17.5 ± 1.6
	$\gamma 2$	17.5 ± 1.6	β	38.6 ± 2.0	α	61.6 ± 2.8	$\delta 1$	13.5 ± 1.8
Leu	$\delta 1/\delta 2$ upfield	23.1 ± 1.3	γ	26.7 ± 1.3	β	42.3 ± 1.9	α	55.6 ± 2.2
	$\delta 1/\delta 2$ downfield	25.7 ± 1.2	γ	26.7 ± 1.3	β	42.3 ± 1.9	α	55.6 ± 2.2

[a] From the "diamagnetic" subset of entries deposited in BioMagResBank (http://www.bmrb.wisc.edu). Values are listed as average ±1 standard deviation. [b] Only aliphatic ^{13}C are considered.

was swept was typically restricted so that the carrier was placed no further than the most downfield resonance of the methyl ^{13}C region.

Data Processing and Analysis. The data were processed with the NMRPipe/NMRDraw software package.[41] Intensities were measured from 3 × 5 data points ($F_1 \times F_2$) centered on the peak maximum. Single-exponential decays were fitted to the data with the experimental error estimated from the standard deviation of the baseline noise. Dispersion profiles were fitted to both a two-parameter model (R_1 and $R_{2,0}$) given by eq 1, and a four-parameter model (R_1, $R_{2,0}$, ϕ, and k_{ex}) given by eqs 1, 2, using simplex routines in MATLAB (The MathWorks Inc.). The statistically significant improvement of the four-parameter fit over that from the two-parameter model was assessed from the F-statistic,[42] with the more complex model considered statistically significant if $p < 0.01$. Errors in fitted variables were estimated from jackknife calculations.

Calculations of Hartmann−Hahn Matching: Database Analysis. As discussed above, the application of a spin-lock field can lead to the coherent transfer of magnetization within the scalar-coupled network of carbon spins in a uniformly ^{13}C-labeled protein sample, with potentially deleterious effects on the quantification of accurate $R_{1\rho}$ relaxation rates. Table 1 presents an overview of the chemical shift distributions in the methyl-containing residues, as calculated from the diamagnetic protein entries in the BioMagResBank (http://www.bmrb.wisc.edu). (Note that those entries having values outside 8 times the standard deviation were removed). It is clear just from inspection of these shift ranges that certain residues will be more susceptible to Hartmann−Hahn matching effects than others. For example, the methyl and Cγ shifts in Leu are proximal so that scalar-coupled magnetization transfer is likely to be much more efficient than for Ala or Thr, where shift differences between one-bond coupled spins are much larger. To quantify this effect, chemical shift differences for every pair of one-, two- and three-bond coupled carbons (where one of the carbons is a methyl) were obtained from Table 1. From these pairwise shift differences the Hartmann−Hahn matching efficiency, A_{HaHa} in eq 3, was calculated for values of ω_1 ranging from 0 to 4.5 kHz and for offsets Ω within ±5 kHz of the methyl, using $^1J_{CC} = 35$ Hz and the values of $^2J_{CC}$ and $^3J_{CC}$ given below and in the subsequent section. Figure 3 shows the resulting contour plots of A_{HaHa}, obtained by treating each one-, two- and three-bond interaction separately.

In the analysis presented, the methyl groups of Val and Leu have been differentiated on the basis of their chemical shifts, i.e., Val/Leu "upfield" or Val/Leu "downfield". For example, it is well-known[43] that the Leu methyl group trans to Cα resonates downfield by several ppm relative to the one that is gauche, in the absence of rotameric averaging around the intervening dihedral angle, χ_2. This distinction is very important, particularly for Leu. First, the two methyl groups experience very different levels of matching with the directly attached Cγ, because the Cγ−Cδ shift difference for the upfield methyl carbon is generally much larger than for the downfield one (the latter is sometimes already in the strong coupling limit in the absence of RF fields). Second, both the three-bond Cα−Cδ scalar-coupling constant and the methyl carbon chemical shift are dependent on the χ_2 angle, and on possible averaging due to motion about the Cβ−Cγ bond. In Figure S1 of Supporting Information it is demonstrated that Leu methyl ^{13}C chemical shifts by themselves are accurate markers of side-chain conformation, so that $^3J_{CC}$ values can be assigned based exclusively on the Leu methyl resonance frequencies. From Figure S1 estimates of 2 and 4 Hz are obtained for $^3J_{CC}$ of methyl carbons with upfield and downfield chemical shifts, respectively.

Calculations of Hartmann−Hahn Matching: Treatment of Experimental Data. Numerical calculations indicate that data points on the $R_{1\rho}$ relaxation dispersion curve that are adversely affected by coherence transfer may be identified in a predictable manner simply from the amplitude of the transfer function, A_{HaHa}, that can be calculated from the assigned side-chain chemical shifts and the scalar-coupling constants between the methyl carbon and other aliphatic carbons. Here (and in the simulations above) we use values of $^1J_{CC} = 35$ Hz, $^2J_{CC} = 1$ Hz, and $^3J_{CC} = 5$ Hz, with the following exceptions and additions based on the literature:[16,44] For Leu methyl groups with a ^{13}C resonance frequency difference in excess of 1 ppm, $^3J_{C\delta C\alpha}$ values given in the previous section were employed, otherwise both ^3J values were assumed to be averaged to 2.0 Hz. In addition, Met $^3J_{C\epsilon C\beta}$ and Val/Leu $^2J_{C\gamma C\gamma}$/$^2J_{C\delta C\delta}$ were set to 3.0 and 0.5 Hz, respectively. Deuterium incorporation induces an isotope shift of the carbon resonance of approximately −0.3 ppm per attached deuteron.[21] Thus, the isotope composition of adjacent carbons that are scalar-coupled to the methyl carbon was also taken into account when evaluating the transfer function, eq 3. Offsets for which A_{HaHa} exceeded 0.01 for any carbon isotopomer (that is either 1-, 2-, or 3-bond removed from the methyl) were excluded from the ensuing analysis (see below).

Results and Discussion

Pulse Sequence. Figure 2 illustrates the $^{13}CHD_2$-selected off-resonance $R_{1\rho}$ pulse sequence that has been used to probe μs time scale dynamics in FKBP12. Briefly, enhanced ^{13}C polarization is generated by a refocused INEPT sequence, and subsequently aligned along an effective field by adiabatic rotation. The spin-locked magnetization is then allowed to relax for a variable period, T, after which it is returned to the z-axis via a second adiabatic pulse. The ^{13}C frequency is labeled during a constant-time period, T_c, and carbon anti-phase coherence is subsequently returned to the ^1H spin, refocused, and detected. Further specific experimental details are given in Materials and

(41) Delaglio, F.; Grzesiek, S.; Vuister, G. W.; Zhu, G.; Pfeifer, J.; Bax, A. *J. Biomol. NMR* **1995**, *6*, 277−293.
(42) Devore, J. L. *Probability and Statistics for Engineering and the Sciences*, 5th ed.; Brooks/Cole Publishing Company: Monterey, California, 1999; p 775.
(43) Bovey, F. *Nuclear Magnetic Resonance Spectroscopy*: Academic Press: San Diego, California, 1988.
(44) Bax, A.; Max, D.; Zax, D. *J. Am. Chem. Soc.* **1992**, *114*, 6923−6925.

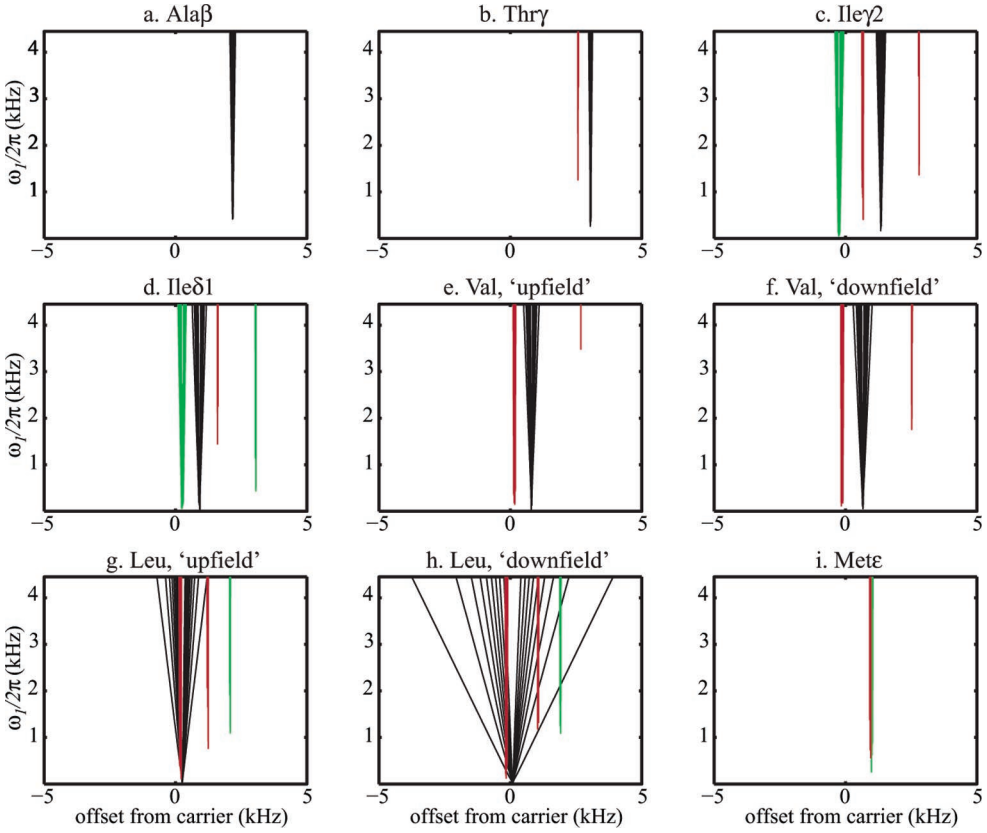

Figure 3. Contour plots of A_{HaHa} calculated as a function of spin-lock offset and field strength, for scalar-coupled methyl groups. The zero frequency offset of the spin-lock carrier is chosen to coincide with the carbon resonance frequency of the evaluated methyl group. Chemical shift differences for the computations were obtained from the BioMagResBank (http://www.bmrb.wisc.edu), as described in the text. Matching due to 1-, 2-, and 3-bond couplings (considered independently) is shown in black, red, and green, respectively. Contour levels are spaced every 10%, from 0.1 to 0.9.

Methods. Due to the editing properties of the refocused INEPT transfer, each methyl group should ideally give rise to a single cross-peak in the 2D spectrum, arising from the $^{13}CHD_2$ isotopomer. In practice, however, it is not possible to completely suppress signals from $^{13}CH_3$ methyl groups, because individual lines of the carbon quartet relax very differently in proteins,[18,45] so that the purging scheme becomes only partially effective.[14] The $^1H-^{13}C$ methyl spectrum of FKBP12 recorded with the present pulse sequence is shown in Figure 4. Despite the effective doubling of the number of cross-peaks, relaxation data could be measured for 42 of the 57 methyl groups in the protein. Overlap precluded the analysis of 13 methyl groups in total, eight of which were already overlapped in the spectrum of the nondeuterated sample and five of which become overlapped with $^{13}CH_3$ isotopomers of different methyl groups. In addition, Ala84β was not observed, presumably due to excessive exchange broadening, and Leu97δ1 is weak in CT-HSQC spectra due to strong coupling between the near-degenerate γ and δ carbon spins.

Measurement of ^{13}C Relaxation Rates in $^{13}CHD_2$ Methyl Groups. As described above, $R_{1\rho}$ relaxation rates were measured for $^{13}CHD_2$ methyl groups of FKBP12. Since $^{13}CH_3$ isotopomers are also present in the 2D spectra, it is possible to measure relaxation rates of these probes as well. As expected, decay curves for $^{13}CH_3$ methyls are not single-exponential (data not shown; see Materials and Methods). In contrast, decay curves measured for $^{13}CHD_2$ were well fitted by single exponentials,

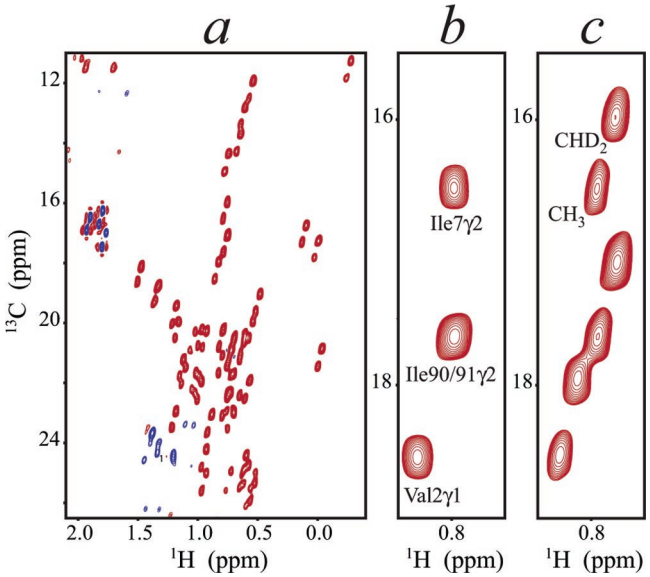

Figure 4. $^{13}CHD_2$-edited HSQC spectrum (500 MHz proton frequency, T = 20 °C), obtained with the pulse sequence of Figure 2, showing the methyl region for 50% deuterated, uniformly ^{13}C-labeled FKBP12 (panel a). A region of the spectrum is enlarged (panel c) and compared to the equivalent region of a nondeuterated sample (panel b).

as shown for Ala64β in Figure 5a−c. However, as discussed in the Theory section, Hartmann−Hahn matching *does* occur under some conditions and strongly influences the time course of the magnetization during the spin-lock period in these cases. This is exemplified by the data for Leu74δ_2 in Figure 5d−f;

(45) Kay, L. E.; Torchia, D. *J. Magn. Reson.* **1991**, *95*, 536−547.

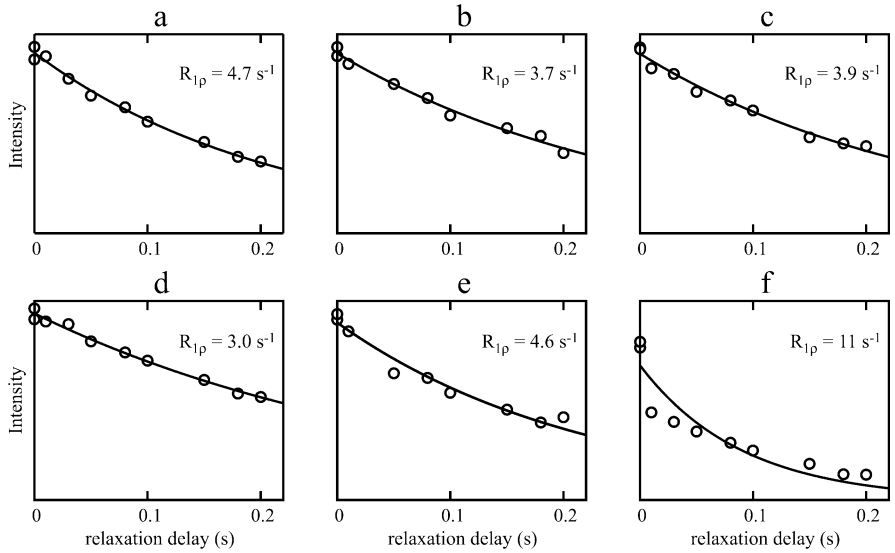

Figure 5. Representative relaxation decays are shown for Ala64β (panels a−c) and for Leu74δ2 (panels d−f) to illustrate the effects of Hartmann−Hahn matching. Data in panels a/d, b/e, and c/f are recorded with the same experimental parameters. Experimental errors are on the order of the size of the symbols. No Hartmann−Hahn transfer is observed for Ala64 (A_{HaHa} < 0.01 in a−c) so that exponential decays are observed in all three cases ($\Omega/2\pi$ = −240, −2740, and −1040 Hz, and θ = 108.7, 121.3, and 114.7°, respectively). In the case of Leu74δ2 Hartmann−Hahn transfer is observed under certain conditions. Panel d, $\Omega/2\pi$ = 595 Hz, $\omega_1/2\pi$ = 708 Hz, θ = 54.5°, no Hartmann−Hahn matching (A_{HaHa} < 0.01); panel e, $\Omega/2\pi$ = −1905 Hz, $\omega_1/2\pi$ = 4511 Hz, θ = 112.9°, with $A_{\mathrm{HaHa}}(^3J_{\mathrm{C}\delta\mathrm{C}\alpha})$ = 0.05; panel f, $\Omega/2\pi$ = −205 Hz, $\omega_1/2\pi$ = 2261 Hz, θ = 95.2°, $A_{\mathrm{HaHa}}(^1J_{\mathrm{C}\delta\mathrm{C}\gamma})$ = 0.81.

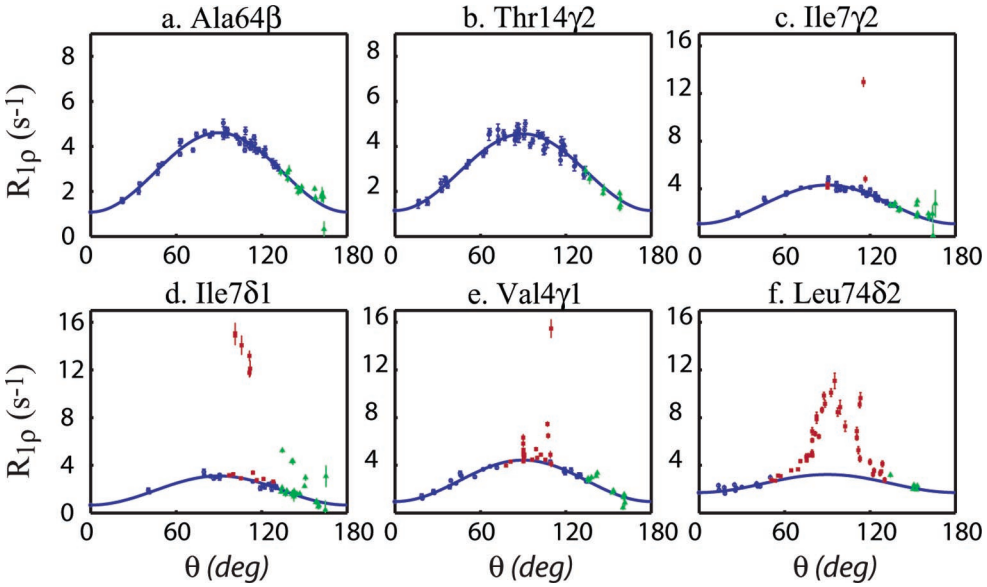

Figure 6. $R_{1\rho}$ relaxation rates, plotted as a function of the tilt angle, θ. Panels a−f show representative curves for different types of methyl-containing residues. a, alanine β; b, threonine γ_2; c, isoleucine γ_2; d, isoleucine δ_1; e, valine γ; f, leucine δ. Blue circles represent data points that were included in the fits, whereas red squares and green triangles indicate data points that were excluded due to Hartmann−Hahn matching and violation of the adiabatic condition, respectively. Due to the periodicity of the tangent function we have chosen the representation 90° ≤ θ ≤ 180° when Ω < 0 and 0° ≤ θ ≤ 90° when Ω > 0. For the present analysis of fast exchange, relaxation rates obtained for any angle θ are equivalent to those obtained for (180° − θ), such that $R_{1\rho}$ relaxation curves are adequately sampled even when the offset carrier frequencies lie predominantly to one side of the resonance. The parameters extracted by model fitting are given in Table 2.

data points become increasingly affected as the matching amplitude, A_{HaHa}, increases from <0.01 (d) to 0.05 (e) to 0.81 (f), leading to erroneous decay rates. Figure 6 shows representative plots of $R_{1\rho}$ relaxation rates as a function of θ for each type of methyl group. From our analysis it is clear that extraction of reliable relaxation rates (blue circles) can be achieved provided that the following two conditions are met. First, satisfactory alignment of the spin magnetization with the effective field requires that $\Omega > -0.9|\omega_1|$ for Ω < 0 (for Ω > 0 alignment is always satisfactory) as we consistently used an increase in the frequency of the RF field during the sweep. Cases where this condition is not fulfilled are readily identified directly from the resonance frequency, $\omega = p_{\mathrm{A}}\omega_{\mathrm{A}} + p_{\mathrm{B}}\omega_{\mathrm{B}}$, of each spin in question along with the experimental parameters ω_1 and ω_{c}, and the associated data should be discarded (green triangles). Second, coherence transfer between the methyl ^{13}C spin and other ^{13}C spins in the side chain or backbone must be insignificant. Potential instances of incorrect $R_{1\rho}$ values can be predicted a priori from eq 3, and the corresponding data points should be excluded from the ensuing analysis (red squares). The occurrence of Hartmann−Hahn matching varies significantly between residue types, depending on the coupling constants and

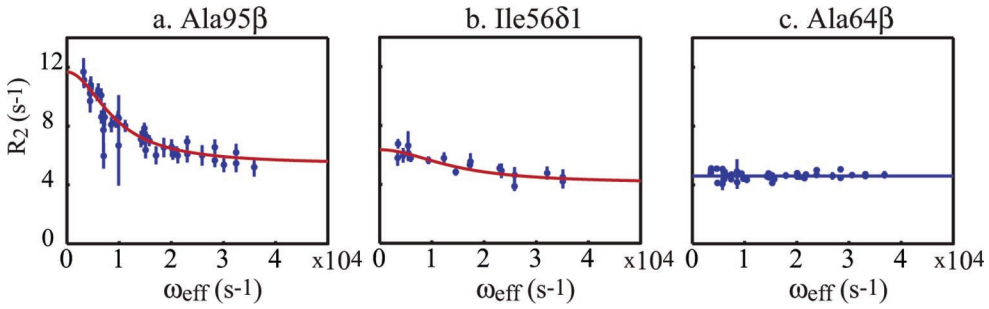

Figure 7. Relaxation dispersion curves, R_2 versus ω_{eff}. Ala95β (a) and Ile56δ1 (b) show significant conformational exchange, with the data well fit to a two-site exchange model (red solid line). Ala64β (c) does not display considerable exchange. Uncertainties in R_2 were obtained from the propagation of errors in $R_{1\rho}$, as follows: $dR_2 = dR_{1\rho}\,[(\Omega^2/\omega_1^2) + 1]$.

chemical shifts of scalar-coupled carbon nuclei. Table 1 lists the chemical shifts of carbons that are one-, two- and three-bond coupled to methyl carbon spins.

It is immediately obvious that Hartmann−Hahn matching is a minor issue for Met, since it does not have a carbon neighboring the methyl group, while it is clearly problematic for Leu since one of the methyls is often directly attached to a carbon nucleus with a very similar chemical shift. As described in some detail in Materials and Methods, data from the BioMagResBank (http://www.bmrb.wisc.edu) were used to calculate the average level of matching expected for the different amino acid types, as a function of the offset and field strength of the RF irradiation, Figure 3. In what follows we will discuss the computational results summarized in Figure 3, along with the experimental data for FKBP12 (Figure 6). $R_{1\rho}$ measurements for Ala (panels a) and Thr (panels b) are largely nonproblematic due to the large shift differences between Cα-Cβ, and between Cγ-Cβ carbons, respectively. Of course, Hartmann−Hahn transfer is still effective in the case where the carrier is placed exactly at the midpoint between the resonance frequencies of the one-bond coupled spins, but this only involves a very small region of the available chemical shift offsets. For Ile, complications may arise for several offsets as a consequence of the many different scalar-couplings involving the methyl groups. Relaxation dispersions for the Cγ2 methyl are typically nonproblematic (panels *c*), because the spin-lock carrier is, in general, not placed between the one-bond coupled Cγ2−Cβ spin pair. In contrast, Hartmann−Hahn matching occurs more often for the Cδ1 group, since placing the carrier near the center of the methyl spectrum results in the unfavorable situation that $\theta_I \approx 180° - \theta_S$ for Cδ1 and Cγ1 (panel d). Still, reliable measurements of $R_{1\rho}$ could be achieved for both methyl groups. Hartmann−Hahn matching occurs for only a few data points for Val methyls where the carrier is positioned almost exactly between the Cγ and Cβ resonance frequencies (Figures 3e−f and 6e). Here, the two methyl groups are distinguished in Figure 3 according to whether their carbon nuclei resonate upfield or downfield, as explained in Materials and Methods. As shown in Figures 3g−h and 6f, the characterization of Leu side-chain dynamics is severely hindered by the small separation in chemical shift between Cδ and Cγ. Indeed, only for methyl groups with a sufficiently upfield shifted carbon nucleus is the Hartmann−Hahn mismatch large enough so that relaxation measurements are not perturbed. As a result only three out of eight nonoverlapping Leu methyl groups in FKBP12 could be analyzed reliably. As expected, $R_{1\rho}$ measurements for Met are free of artifacts, as the methyl group has no directly attached carbon atom, and the only significant long-range coupling occurs between the Cϵ and Cβ nuclei, which have a large chemical shift separation (Figure 3i).

Analysis of Dispersion Profiles. The presence of slow motions at methyl sites in FKBP12 was established by comparison of the goodness of two (R_1 and $R_{2,0}$)- and four (R_1, $R_{2,0}$, ϕ, and k_{ex})-parameter fits to the measured relaxation rates using *F*-test statistical criteria. A statistically significant improvement of the fit at the 99% confidence level was taken to indicate that the methyl group in question does indeed undergo conformational exchange between different magnetic environments. Once R_1 has been determined by curve fitting it is possible to represent the data in Figure 6 in an alternative fashion that plots $R_2 = R_{1\rho}/\sin^2\theta - R_1/\tan^2\theta = R_{2,0} + R_{ex}$ as a function of ω_{eff} (Figure 7). In these plots, it is easier to visualize exchange contributions, which appear as dispersions superposed on B_1 field-independent contributions due to dipolar and CSA contributions.

Flat profiles were obtained for 24 out of the methyl groups that could be characterized in FKBP12, indicating that motional processes could not be detected at these sites. In contrast, μs time scale dynamics were observed for 12 methyl sites, for which the data were successfully modeled assuming two-state exchange, eq 2, with $p < 10^{-2}$. The complete set of curves is shown in Figure S2 (Supporting Information). Figure 7a shows the dispersion profile for Ala95β, with a sizable contribution from conformational exchange. As exemplified for Ile56δ1 (Figure 7b), variations in both ω_1 and Ω allow coverage of a large effective field range, such that exchange can still be quantified reliably even though a large fraction (approximately two-thirds) of the experimental data points were discarded due to Hartmann−Hahn matching, or violation of the adiabatic condition. Figure 7c shows the results for a residue (Ala64β) that is not affected significantly by exchange broadening.

Table 2 lists the individually optimized exchange parameters for the methyl groups that experience conformational exchange in FKBP12. Individual fits produced values of k_{ex} ranging between $(4.4-14.5) \times 10^3\ s^{-1}$, with $\langle k_{ex}\rangle = (8.6 \pm 3.5) \times 10^3\ s^{-1}$. Since the optimized parameters are interdependent, these variations are not necessarily significant.[3,46] To establish whether the observed dispersions are the result of a global exchange process we simultaneously fitted all of the relaxation profiles (i.e. from all exchanging methyl groups) to yield a global k_{ex} rate and methyl-specific parameters[3] R_1, $R_{2,0}$, and ϕ. In this case $k_{ex} = (7.9 \pm 1.0) \times 10^3\ s^{-1}$, the fitted parameters are listed in Table S2 (Supporting Information). For the 12 residues that

(46) Ishima, R.; Torchia, D. *J. Biomol. NMR* **1999**, *14*, 369−372.

Table 2. Exchange Parameters for Methyl Groups Extracted from $R_{1\rho}$ Relaxation Dispersion Curves

residue	k_{ex} (10^3 s^{-1})	$p_a p_b \Delta\omega^2$ (10^3 s^{-2})	R_1 (s^{-1})	$R_{2,0}$ (s^{-1})	χ_ν^2	p-value[a]	$R_{ex}(\omega_{eff} \rightarrow 0)$($s^{-1}$)
Thr6γ2	4.4 ± 2.6[b]	6.1 ± 2.0	2.02 ± 0.10	5.0 ± 0.1	1.28	2.8×10^{-6}	1.4
Val24γ2	6.6 ± 4.6	19 ± 8.1	1.32 ± 0.39	5.4 ± 0.4	2.46	5.8×10^{-8}	2.9
Ile56δ1	14.4 ± 8.4	33 ± 32	0.69 ± 0.16	4.1 ± 0.8	1.12	1.0×10^{-5}	2.3
Val63γ2	4.9 ± 4.2[b]	8.0 ± 6.4	0.75 ± 0.05	4.3 ± 0.4	2.14	9.4×10^{-5}	1.6
Thr75γ2	8.2 ± 5.9	5.5 ± 3.3	1.06 ± 0.01	4.8 ± 0.1	1.94	5.7×10^{-3}	0.7
Ile76γ2	9.5 ± 1.7	138 ± 22	3.67 ± 0.10	8.0 ± 0.9	0.95	$<1 \times 10^{-10}$	14.6
Ala81β	4.8 ± 2.1	14 ± 2.0	1.74 ± 0.12	5.4 ± 0.1	2.51	$<1 \times 10^{-10}$	3.0
Ile90δ1	9.0 ± 2.6	19 ± 5.4	0.59 ± 0.26	2.6 ± 0.3	1.43	$<1 \times 10^{-10}$	2.1
Ile91δ1	12.0 ± 4.2	37 ± 19	0.78 ± 0.61	2.3 ± 0.9	1.89	4.0×10^{-6}	3.1
Ala95β	9.1 ± 1.1	57 ± 7.5	1.07 ± 0.34	5.4 ± 0.3	1.12	$<1 \times 10^{-10}$	6.3
Thr96γ2	5.8 ± 1.4	27 ± 3.6	1.48 ± 0.19	5.7 ± 0.2	1.89	$<1 \times 10^{-10}$	4.6
Val101γ2	14.5 ± 5.0	24 ± 11	1.14 ± 0.22	4.2 ± 0.3	2.16	1.7×10^{-6}	1.7

[a] Probability that the improvement in the fit obtained by including two-state fast-exchange in the model, eqs 1,2, is due to chance. [b] These uncertainties were obtained from 200 Monte Carlo simulations, as jack-knife estimates did not converge.

sense conformational dynamics the average reduced χ^2 value, $\langle\chi_\nu^2\rangle$, increased by only 1.1% in the group fit relative to $\langle\chi_\nu^2\rangle$ for the individual fits, while reducing the number of fitting parameters for each residue from four to three. Also, for none of the residues did χ_ν^2 increase by more than a factor of 2. This good fit to the combined data suggests that the exchange contributions may be due to a single large-scale conformational rearrangement.[3]

The residue specific ϕ parameters are a product of the populations and the chemical shift difference between the exchanging sites, eq 2. Thus, the site-specific chemical shift differences between these states are proportional to the square root of ϕ. Since the product of the populations has an upper limit of 0.25, we derive a lower limit for the chemical shift difference, $\Delta\delta_{low} = 2\phi^{1/2}/\omega_c$ (in ppm). For the methyl carbons in Table 2 $\Delta\delta_{low}$ ranges between 0.19 ppm (for Thr75γ2) and 0.95 ppm (for Ile76γ2). Although translating extracted chemical shift differences into structural restraints is far from trivial,[5,47−49] large changes are consistent with significant structural differences between states.

Conformational Transition Dynamics of FKBP12. Figure 8a illustrates the location of all methyl groups in the FKBP12 structure for which relaxation data could be obtained. As observed, these probes are distributed throughout the entire molecule. The methyl groups are color coded according to the $\Delta\delta_{low}$ from the group fit, as detailed in the legend. Figure 8b highlights the location of the tight-binding immunosuppressant drug FK-506. Binding of immunosuppressants and peptides to FKBP12 occur in the same active-site pocket, with the pipecolinyl ring of FK-506 mimicking the proline ring of the peptide substrate.[50,53] This functional center is localized to a shallow cavity between the α-helix and the β-sheet, with its base formed by Trp59. Five residues that form hydrogen bonds or other close contacts to FK-506 or rapamycin contain methyl groups (Val55, Ile56, Ala81, Ile90, and Ile91),[51,53,54] and their dynamics can

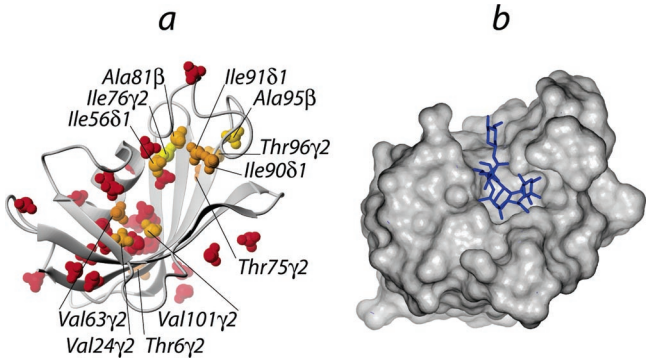

Figure 8. Three-dimensional structures of FKBP12. Panel a shows the structure of the free protein (PDB accession number 1FKS[50]). The backbone is represented as a ribbon, with space-filling representation for the 37 methyl groups for which $R_{1\rho}$ relaxation dispersion data was measured. The methyl atoms are color coded according to the lower limit chemical shift difference between the two exchanging states. Residues with no exchange detected are red; thereafter dark orange, $0 < \Delta\delta_{low} < 0.25$ ppm; light orange, $0.25 < \Delta\delta_{low} < 0.50$ ppm; gold, $0.50 < \Delta\delta_{low} < 0.75$ ppm; and yellow $\Delta\delta_{low} > 0.75$ ppm. In panel b FKBP12 is shown bound to FK-506 (PDB accession number 1FKJ[51]). The protein is shown as a space-filling model, with the bound inhibitor in stick representation. Figure prepared with Molmol.[52]

be studied with the present method; Ile56, Ala81, Ile90, and Ile91 were all found to be dynamic in the absence of ligand. Residues undergoing conformational exchange are also proximal to the binding surface identified for 2-phenylimidazole, that was mapped by chemical shift perturbation of the methyl groups of Val24, Leu50, Val55, Ile56, Val63, Ile76, and Ile90 upon addition of drug.[19] Of interest, the active site region responsible for proline isomerase activity[55] also serves as the binding surface for the type I TGFβ receptor,[56] while loop residues His87-Ile90 and the segment Asp37-Phe46 are involved in the recognition of calcineurin.[57] In addition, the FKBP12 active site interacts with tissue-specific calcium-release channels.[58] Clearly, the ability of FKBP12 to function as an isomerase enzyme, as a modulator of immune response, and as a component of receptor heterocomplexes depends on its extensive plasticity. The residues for which conformational exchange was quantified (see Table 2) are generally conserved among small FKBPs,[59] suggesting their structural and functional significance. It has

(47) Evenäs, J.; Malmendal, A.; Akke, M. *Structure* **2001**, *9*, 185−195.
(48) Volkman, B. F.; Lipson, D.; Wemmer, D. E.; Kern, D. *Science* **2001**, *291*, 2429−2433.
(49) Grey, M. J.; Wang, C.; Palmer, A. G. *J. Am. Chem. Soc.* **2003**, *125*, 14324−14335.
(50) Michnick, S.; Rosen, M.; Wandless, T.; Karplus, M.; Schreiber, S. *Science* **1991**, *252*, 836−839.
(51) Wilson, K.; Yamashita, M.; Sintchak, M.; Rotstein, S.; Murcko, M.; Boger, J.; Thomson, J.; Fitzgibbon, M.; Black, J.; Navia, M. *Acta Crystallogr., Sect. D* **1995**, *51*, 511−521.
(52) Koradi, R.; Billeter, M.; Wüthrich, K. *J. Mol. Graphics* **1996**, *14*, 51−55.
(53) Van Duyne, G.; Standaert, R.; Karplus, P.; Schreiber, S.; Clardy, J. *Science* **1991**, *252*, 839−842.
(54) Sich, C.; Improta, S.; Cowley, D.; Guentet, C.; Merly, J.-P.; Teufel, M.; Saudek, V. *Eur. J. Biochem.* **2000**, *267*, 5342−5354.
(55) Timerman, A.; Wiederrecht, G.; Marcy, A.; Fleischer, S. *J. Biol. Chem.* **1995**, *270*, 2451−2459.
(56) Huse, M.; Chen, Y.-G.; Massagué, J.; Kuriyan, J. *Cell* **1999**, *96*, 425−436.
(57) Griffith, J.; Kim, J.; Kim, E.; Sintchak, M.; Thomson, J.; Fitzgibbon, M.; Fleming, M.; Caron, P.; Hsiao, K.; Navia, M. *Cell* **1995**, *82*, 507−522.
(58) Schiene-Fischer, C.; Yu, C. *FEBS Lett.* **2001**, *495*, 1−6.
(59) Galat, A. *Eur. J. Biochem.* **2000**, *267*, 4945−4959.

been noted that 11 residues are completely conserved among 16 species variants of FKBP12 and among 11 variants of FKBP13.[59] Five of these (Ile56, Leu74, Tyr82, Leu97 and Phe99) have bulky, hydrophobic side chains, and Ile56, Tyr82, and Phe99 are directly involved in the binding of FK-506. The two leucines are more internal, but play an important structural role in shaping the binding pocket: Leu74 interacts with Val2, Trp59, and Val101, whereas Leu97 bridges between Tyr82, Ile91, and Ile56. Perhaps somewhat surprisingly, the remaining six strictly conserved residues in FKBP12 are all glycine (residues 10, 19, 58, 62, 69, and 83), dispersed throughout the structure, and not *directly* implicated in recognition. Since glycine residues lack a side chain, they often introduce flexibility to protein structures. This plasticity is important for function and may have been preserved to enable FKBP12 to present alternative hydrophobic interaction surfaces, necessary for the recognition of a variety of targets.

Employing Alternative Schemes for Obtaining $^{13}CHD_2$ Methyl Groups in Proteins. The methodology presented here can be further adapted for other applications. Sensitivity can be improved by increasing the amount of deuterium in the growth media to above the 50% that was used in the current study. In the case of larger proteins, where resonance overlap is limiting, it may be advantageous to pursue other labeling schemes that make clever use of bacterial biosynthesis pathways to tailor ^2H and ^{13}C enrichment. Viable approaches that mitigate coherent magnetization transfer between carbons and optimize the level of the desired $^{13}CHD_2$ isotopomer include the use of (i) protonated 3-^{13}C-pyruvate[60] in deuterated solvent,[14] (ii) chemically synthesized $^{13}CHD_2$-valine[61] or (iii) a D_2O cell culture medium containing 3-^{13}C-pyruvate, 50−60% deuterated at the 3-position, and 4-^{13}C 2-ketobutyric acid, 98% and 62% deuterated at the 3- and 4-positions, respectively.[62] More recently, both 2-ketobutyrate and 2-keto-isovalerate with $^{13}CHD_2$ label have become available commercially.[63] Addition of the precursors approximately 1 h prior to induction in a protein expression system based on U-^2H-glucose and D_2O produces proteins where the Ile(δ1), Leu and Val methyl groups are of the $^{13}CHD_2$ variety. This strategy generates proteins with greatly simplified spectra and with reduced resonance overlap. $^{13}C-^{13}C$ couplings are absent, with the exception of the very small two-bond interaction between the methyl carbons of Val and Leu, and the methyl groups are embedded in a highly deuterated background, with strongly reduced dipolar relaxation.

Concluding Remarks

Protein samples uniformly labeled with ^{13}C and randomly, fractionally labeled with ^2H, can be prepared in a straightforward fashion and at moderate cost to investigate protein internal dynamics. These samples are suitable for ^2H relaxation studies of picosecond to nanosecond dynamics, and—as shown here—are also valuable for the analysis of slower (μs) motions at methyl side-chain positions that escape detection by CPMG-based methods. Here an off-resonance rotating-frame relaxation method is presented for the quantitative study of μs time scale dynamics. Calculations and experiment demonstrate that Hartmann−Hahn matching for *J*-coupled spins in uniformly ^{13}C-enriched proteins is easily predicted, so that $R_{1\rho}$ relaxation dispersion curves can be measured reliably for the majority of methyl groups. The technique was applied to FKBP12, and small, but significant, exchange contributions were measured for many methyl ^{13}C nuclei. A two-state model was sufficient to describe the dynamic process at the level of individual sites in the protein. The relaxation data for all methyl groups with conformational exchange could be fit nicely to a global exchange process, strongly suggesting that the FKBP12 molecule as a whole switches between different conformational states in the absence of ligand. The methyl groups showing conformational exchange cluster in functionally important regions, strongly suggesting that the observed conformational dynamics are important for function, as reported for other systems.[4,6,64]

Acknowledgment. We thank Drs. Michael Rosen (UT Southwestern, Dallas) and Timothy Logan (NHMFL, Tallahassee) for FKBP12 clones, Dr. Patrik Lundström for the global optimization program, and Eva Thulin and Hanna Nilsson for assistance with protein expression and purification. Drs. Ad Bax (NIH) and Ranjith Muhandiram (University of Toronto) are acknowledged for providing the scalar-coupling data used in this paper. This work was supported by the Swedish Research Council, the Swedish Foundation for Strategic Research (M.A.), and by the Canadian Institutes of Health Research (L.E.K.). L.E.K. holds a Canada Research Chair in Biochemistry. F.A.A.M. was supported by a Marie-Curie fellowship awarded by the European Commission (HPMF-CT-2001-01245).

Supporting Information Available: One figure showing the correlation of Leu methyl ^{13}C chemical shift differences with $^3J_{C\delta C\alpha}$, one figure showing the dispersion profiles for all methyl groups subject to chemical exchange in FKBP12, one table with the values for offset and field strength used in the off-resonance $R_{1\rho}$ experiment, and one table with the parameters obtained from the combined fit of the experimental data to a global two-state process. This material is available free of charge via the Internet at http:/pubs.acs.org.

JA0570279

(60) Lee, A.; Urbauer, J.; Wand, A. *J. Biomol. NMR* **1997**, *9*, 437−440.
(61) Chaykovski, M.; Bae, L.; Cheng, M.-C.; Murray, J.; Tortolani, K.; Zhang, R.; Seshadri, K.; Findlay, J.; Hsieh, S.-Y.; Kalverda, A.; Homans, S.; Brown, J. *J. Am. Chem. Soc.* **2003**, *125*, 15767−15771.
(62) Ishima, R.; Louis, J.; Torchia, D. *J. Biomol. NMR* **2001**, *21*, 167−171.
(63) Tugarinov, V.; Ollerenshaw, J.; Kay, L. *J. Am. Chem. Soc.* **2005**, *127*, 8214−8225.
(64) Feher, V.; Cavanagh, J. *Nature* **1999**, *400*, 289−93.